# Geochronological constraints on the genesis of high-grade iron ore in the Gongchangling BIFs from the Anshan-Benxi area, North China Craton

Xiao-Hui Sun[a,*], Hao-Shu Tang[b,*], Yan Luan[a], Ji-Hong Chen[c]

[a] School of Earth Science and Resources, Chang'an University, Xi'an 710054, China
[b] State Key Laboratory of Ore Deposit Geochemistry, Institute of Geochemistry, Chinese Academy of Sciences, Guiyang 550081, China
[c] Gongchangling Mining Company Limited of Anshan Iron and Steel Group Mining Company Limited, Liaoyang 111007, China

## ARTICLE INFO

## ABSTRACT

The Gongchangling iron deposit located in the northeast of the North China Craton is hosted in late Neoarchean Algoma-type BIFs. It is famous for the major production of high-grade iron ore in the Gongchangling No.2 mining area in China. With regard to the genesis of high-grade iron ore, more and more evidences indicate that it was related with hydrothermal enrichment of BIFs. However, the hydrothermal nature was argued for meteoric, metamorphic or migmatitic fluid. In this study, the trace element compositions of garnet from the altered wall-rock of high-grade iron ore obtained by LA–ICP–MS show compositional zoning, indicating it is a metamorphic origin. These garnets yield a Sm–Nd isochron age of 1888 $\pm$ 77 Ma, interpreted as the time of metamorphism in this area. LA–ICP–MS U–Pb dating of zircon from the upper migmatite zone shows that the migmatitic granite was formed at 2478 $\pm$ 36 Ma. Since the REE patterns of garnet suggest that it was formed in the nearly neutral fluid rather than the acid meteoric fluid in the Paleoproterozoic. Hence, combined the ages of metamorphism and migmatization with high-grade iron ore of 1840 $\pm$ 7 or 1860 $\pm$ 7 Ma obtained by previous studies, it indicates that the genesis of the high-grade iron ore derived from the enrichment of BIFs by metamorphic hydrothermal fluid.

## 1. Introduction

Banded iron formations (BIFs) are a unique type of Precambrian marine chemical sedimentary rock (Bekker et al., 2010; Chen and Zhao, 1997; Chen et al., 1994; James, 1954; Moon et al., 2017; Tong et al., 2019; Yang et al., 2015, 2018; Zhang et al., 2012). BIFs are broadly defined as being either Algoma-type or Superior-type based on depositional environment, the former were apparently formed close to volcanic arcs and spreading centers, and produced by exhalative hydrothermal processes related to submarine volcanism. While the latter were developed in passive-margin, sediment-dominated settings (Gross, 1980; Huston and Logan, 2004; Klein, 2005; Konhauser et al., 2009, 2017).

Generally, the BIFs-related high-grade iron ores are mainly composed of martite and hematite, and attributed to hypogene process and supergene hydrothermal enrichment of BIFs in general (Bekker et al., 2010; Clout, 2006; Egglseder et al., 2017; Figueiredo e Silva et al., 2013; Hagemann, et al., 2016; Lascelles, 2012; Spier et al., 2008; Thorne et al., 2009). However, the BIFs-related high-grade iron deposits in China (total Fe $\geq$ 50%) exhibit different geological characteristics

compared to those of the world, which are mainly composed of magnetite and occur in the greenstone belt (Li et al., 2015; Wang et al., 2014; Zhai and Santosh, 2013).

In China, BIFs are mainly distributed in the North China Craton (NCC) (Hou et al., 2019; Li et al., 2014a,b; Wan et al., 2012a; Zhang et al., 2014). The Gongchangling iron deposit in the Anshan-Benxi area, northeast of the NCC, is hosted in the oxide facies Algoma-type BIFs. And the Gongchangling No. 2 mining area represents the largest and most typical BIFs-related high-grade iron ore distribution area in China (Han et al., 2014; Li et al., 2014a, 2015; Sun et al., 2014a, 2018; Wang et al., 2012, 2013, 2014; Zhou, 1994). More and more studies suggest that desilicification process has been considered as the principal mechanism for generating the high-grade iron ores from the Gongchangling No.2 mining area (Li et al., 2015; Sun et al., 2018; Wang et al., 2014). During this process, the silica of BIFs was leached out by the hydrothermal fluid, while the magnetite of BIFs was reserved to form the high-grade iron ores. However, as for the nature of the hydrothermal fluid, there are three distinctively different viewpoints containing migmatitic hydrothermal fluid from magma (Chen et al., 1985; Cheng, 1957; Li et al., 1977; Li et al., 2014a; Zhao and Li, 1980; Zhao

et al., 1979), metamorphic hydrothermal fluid generated by regional metamorphism (Guan, 1961; Liu and Jin, 2010; Shi and Li, 1980; Sun et al., 2014a, 2018; Wang et al., 2014; Zhou, 1994), and meteoric fluid driven by extensional tectonics (Li, et al., 2014c; Li, et al., 2015; Li, et al., 2019).

In this paper, we determined the trace element composition of garnet from the altered wall-rock of the high-grade iron ore by laser ablation inductively coupled plasma mass spectrometry (LA–ICP–MS). It indicates that the garnet was formed under neutral condition during prograde metamorphism. Therefore, we can use these garnets for the direct Sm–Nd isotopic dating to determine the age of metamorphism. Meanwhile, we present the age of migmatization by zircon U–Pb dating of the migmatitic granite from the Gongchangling No.2 mining area. Compared with previous studies, these data will enable us to constrain the genesis of the high-grade iron ore in the Gongchangling No.2 mining area from the Anshan-Benxi area, northeast of the NCC.

## 2. Geological background

### 2.1. Regional geology

As one of the oldest cratonic blocks in the world, the North China Craton consists of uniform Archean to Paleoproterozoic basement overlain by Mesoproterozoic to Cenozoic cover (Song et al., 1996; Zhao and Zhai, 2013). The Archean basement in the NCC was formed during two distinct periods: 2.8–2.7 Ga and 2.6–2.5 Ga, of which the former is considered as a major period of juvenile crustal growth in the NCC, while the latter is related to the underplating of mantle-derived magma (Zhao and Zhai, 2013). Three Paleoproterozoic orogenic belts have been identified in the NCC, named the Trans-North China Orogen (TNCO), Khondalite Belt and Jiao-Liao-Ji Belt (JLJB), respectively (Fig. 1). The EW-trending Khondalite Belt was formed by the collision between the Yinshan Block and the Ordos Block at ~1.95 Ga to form the Western Block of the NCC (Zhao et al., 2003). Likewise, the NE-SW trending Jiao-Liao-Ji Belt was formed by the collision between the Longgang Block in the north and Langrim Block in the south at ~1.90 Ga to form the Eastern Block (Zhao et al., 1998, 2012). Then the Eastern Block collided with the Western Block along the TNCO at ~1.85 Ga to form the coherent basement of the NCC (Zhao et al., 2001, 2003, 2005).

The Longgang Block is bounded by the JLJB in the southeast and the TNCO in the northwest (Fig. 1a), and consists of an Archean metamorphic basement overlain by Neoproterozoic–Paleozoic sedimentary strata. The metamorphic basement is characterized by abundant late Archean tonalite-trondhjemite-granodiorite (TTG) suites and a minor amount of supracrustal rocks. It is one of the oldest continental nuclei on earth as a consequence of its preservation of the oldest rock in the Anshan area ranging up to ~3.8 Ga (Song et al., 1996). Moreover, Cui et al. (2013) reported the first occurrence of a xenocrystic zircon with age of ca. 4.17 Ga from late Archaean amphibolites in the Benxi Archean supracrustal greenstone belt, which is close to above 3.8 Ga rocks.

The JLJB separates the Longgang and Langrim Blocks. It mainly consists of metavolcano-sedimentary successions and granitic to mafic intrusions that were metamorphosed to greenschist–amphibolite facies. The tectonic nature of the JLJB is still controversial, including arc-continent collision (Bai, 1993; Faure et al., 2004; Li et al., 2017) and intra-continental rift (Li and Zhao, 2007; Peng and Palmer, 1995; Wang et al., 2017; Zhang and Yang, 1988). Zhao et al. (2012) complied different events from the two models into an integrated progressive tectonic process and proposed the rift-and-collision model. It indicates that the JLJB underwent extensional setting and rift in the period 2.2–1.9 Ga, leading to the opening of an incipient ocean that broke the Eastern Block into two small blocks (Longgang and Langrim Blocks). At ~1.9 Ga, the two blocks were re-assembled through subduction and collision to form the Jiao-Liao-Ji Belt (Zhao et al., 2012; Zhao and Zhai,

2013). Geochronological data show that most of the metasedimentary-metavolcanic successions in the JLJB formed during 2200–2100 Ma, and then were metamorphosed and deformed from 1950 to 1850 Ma (Liu et al., 2018; and references therein).

The Anshan-Benxi area, Liaoning Province, with 20% total reserves of iron ore in China, is located in the Longgang Block adjacent to the JLJB, northeast margin of the NCC (Li et al., 2014b; Wang et al., 2014; Xu et al., 2019). The early Precambrian metamorphic rock series are composed of the Archean Anshan Group and the Paleoproterozoic Liaohe Group in this area, and both the Anshan and Liaohe Groups are overlain unconformably by the undeformed Neoproterozoic Sinian sediments (Tang et al., 2013a,b). The Neoarchean Anshan Group comprises a supracrustal sequence that was intruded by the granitic gneisses (the Anshan gneisses), resulting in the supracrustals occurred as lenses of variable sizes within the gneisses (Zhai and Windley, 1990; Zhai et al., 1990a). The main rock types of the Anshan Group consist of amphibolites, biotite leptynites (fine grained biotite-plagioclase gneiss), schists, migmatites, BIFs, siliceous rocks and carbonates on the whole, and had undergone greenschist to amphibolite facies metamorphism (Zhai et al., 1990b; Zhou, 1994). The Anshan Group is divided into the Cigou, Dayugou and Yingtaoyuan Formations from bottom to top. Recent geochronological studies in the Anshan-Benxi area indicate that the forming age of the Anshan Group BIFs is late Neoarchean (Dai et al., 2014; Tong et al., 2019; Wan et al., 2012a). Granitic rocks are widely distributed in the Anshan-Benxi area, and most of these rocks had undergone migmatization (Fig. 1; Li et al., 2015). The BIFs-related high-grade iron deposits in the Anshan-Benxi area are mainly distributed in the Gongchangling, Qidashan, Nanfen and Wangjiabuzi. Among them, the Gongchangling ore field is the largest and most typical one (Wang et al., 2014).

### 2.2. Ore deposit geology

The Gongchangling iron ore field in the Anshan-Benxi area comprises the Nos. 1–3 and Laoling-Bapanling mining areas with proven ore reserves of 1583 million tonnes (Mt) (Chi, 1993; Zhou, 1994; Li et al., 2015). The Gongchangling No.2 mining area is located in the north limb of the Gongchangling anticline. It has proven ore reserves of 946 Mt, including 782 Mt low-grade and 164 Mt high-grade iron ores, which provided with the largest high-grade iron ore reserves in the Anshan-Benxi area (Li et al., 2015). It is bounded by the Hanling Fault to the northwest, the Pianling Fault to the southeast, and is adjacent to the Laoling-Bapanling mining area (Fig. 2). The iron ore-bodies in the Gongchangling No.2 mining area are ca. 4500 m in length and 300–600 m in width. It is hosted by the metamorphic rock series of the Cigou Formation of the Anshan Group. These rocks occur as elongated enclaves within the granitic rocks with dipping NE at the angle of 60 to 85 degrees. There are six layers of BIFs in the Gongchangling No.2 mining area, and the average total Fe grade of BIFs is 33.72% (Li et al., 2015). A brief description of the rock units is given as follows from base to top (Fig. 3): (1) Lower amphibolite zone; (2) Lower schist zone; (3) Lower iron ore belt: composed of the first layers of BIFs (Fe1, Fe1–Fe6 means the first to the sixth layer of BIFs), middle schist and Fe2; (4) Middle biotite leptynite zone: interlayer with Fe3, and considered as the key marker layer in distinguishing the lower and upper iron ore belts; (5) Upper iron ore belt: consists of the Fe4, lower amphibolite, Fe5, upper amphibolite and Fe6. Most of the high-grade magnetite ores are hosted in the Fe6, accounting for 77.1% of the total high-grade iron ore reserves in the Gongchangling No.2 mining area; (6) Siliceous strata. Both the hanging wall and footwall rocks of the iron-bearing series are migmatitic granite, including the Gongchangling granite (lower migmatite zone (ML)) and the Mayu granites (upper migmatite zone (Mu), Fig. 3) (Wan, 1994; Li et al., 2015).

The mode of occurrence of the high-grade iron ores is roughly consistent with that of BIFs, and there is a smooth transition from high-grade iron ores to BIFs (Fig. 4a). The iron ores are mainly characterized
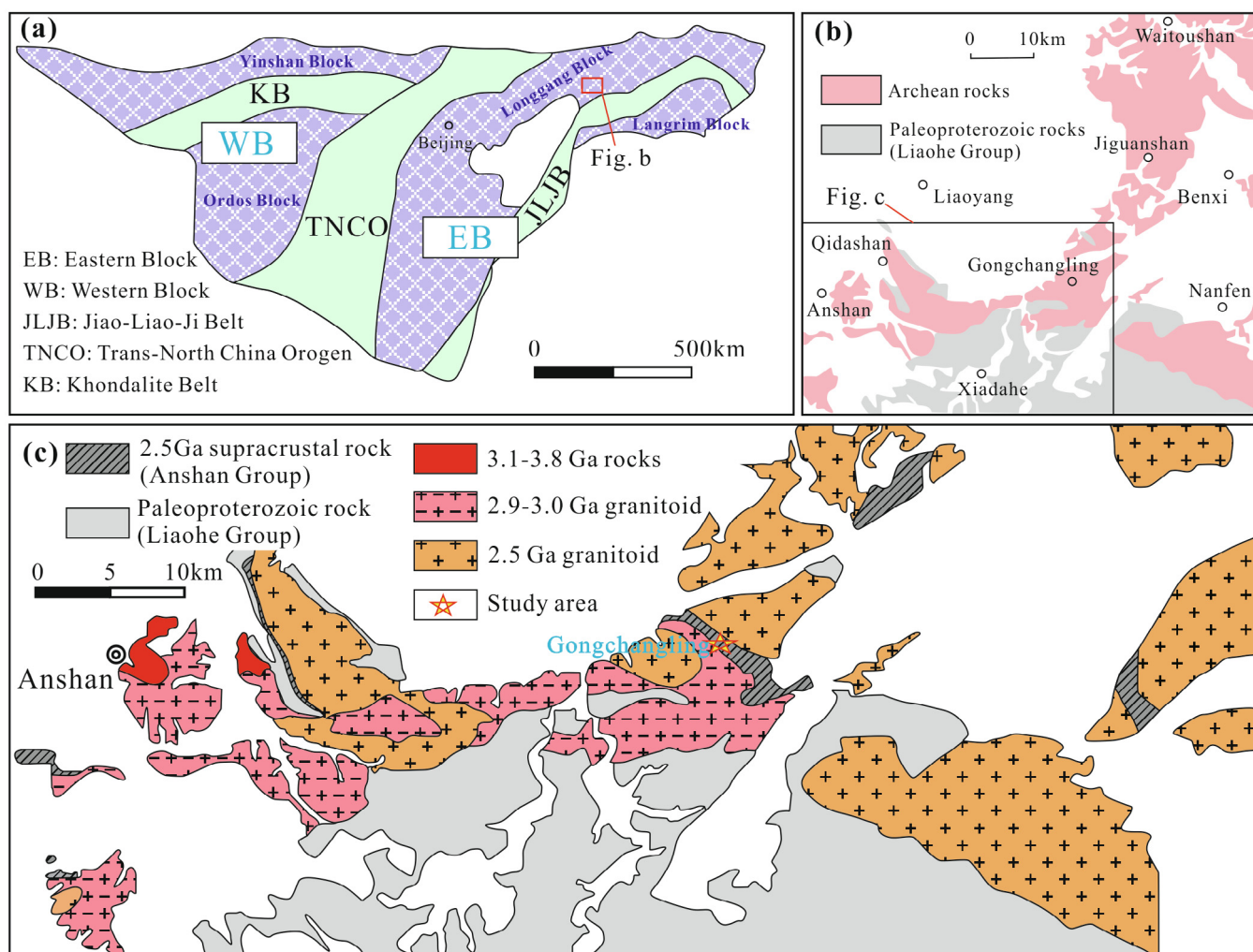
**Fig. 1.** Geological map of the Anshan-Benxi area, Liaoning Province (modified after Dong et al., 2017; Wan et al., 2016; Zhao and Zhai, 2013).

by banded (BIFs) or massive (high-grade iron ore) structure and granular texture. The iron ores are divided into four types: i) low-grade magnetite ore with ore mineral of magnetite and gangue minerals of quartz, actinolite, chlorite, biotite and apatite; ii) low-grade martite ore with ore minerals of specularite, martite, minor magnetite and limonite; and the gangue minerals are similar to those of the low-grade magnetite ore; iii) high-grade magnetite ore with ore minerals of magnetite and

minor hematite; and gangue minerals of quartz, garnet, cummingtonite, chlorite and calcite; iv) high-grade hematite ore with ore mineral of specularite; and gangue minerals are similar to those of the high-grade magnetite ore.

Strike reverse faults and transverse faults are well developed in this area. The occurrence of high-grade iron ores is mainly controlled by the strike reverse faults which formed during regional metamorphism along
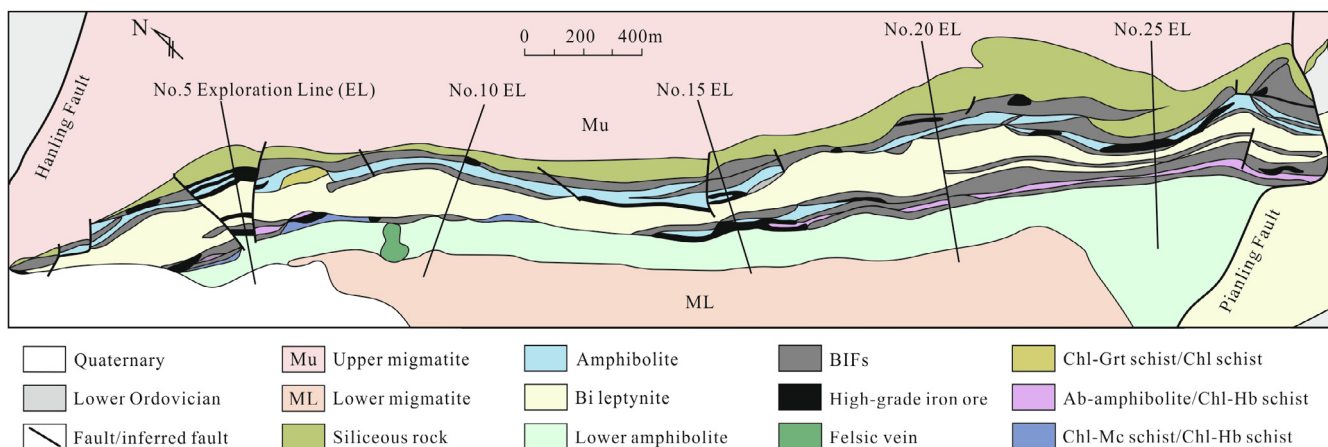


**Fig. 2.** Geological map of the Gongchangling No.2 mining area (modified after Zhou, 1994).
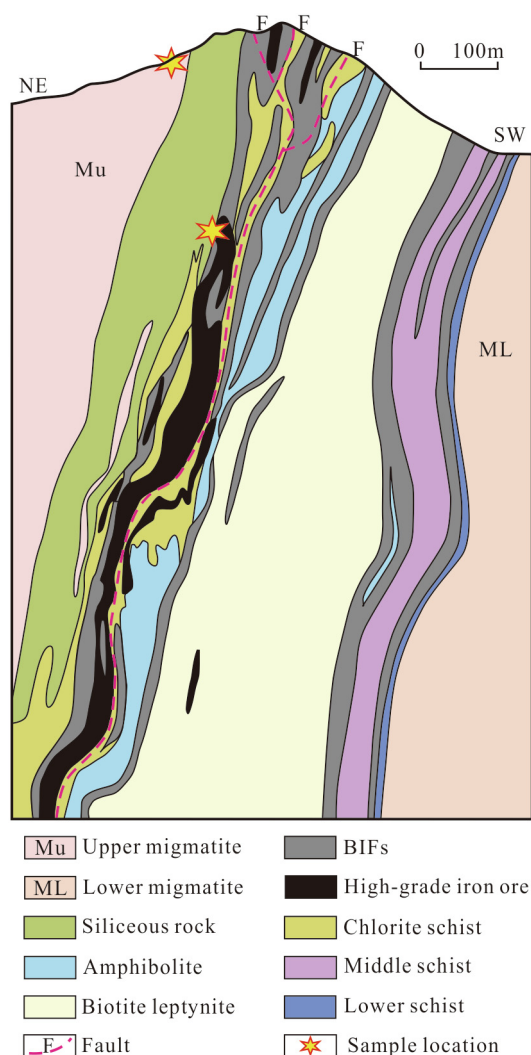
3

**Fig. 3.** Geological cross-section of the Gongchangling No.2 mining area (after Chi, 1993; Zhou, 1994).

the ore layer of Fe6, while the transverse faults formed after mineralization period (Zhou, 1994).

All the ore-bodies are consistent with the occurrence of wall-rocks. The wall-rocks of high-grade iron ores exhibit obvious alteration zoning in sequence of amphibolization (actinolitization and cummingtonite), garnetization and chloritization outwards from the ore-bodies. The scale of high-grade iron ores is roughly proportional to alteration intensity of wall-rocks in general (Zhu et al., 2016).

## 3. Sampling and analytical methods

### 3.1. Sample description

Garnet is widely distributed in the Gongchangling No.2 mining area. It is abundant in the altered wall-rocks while minor in the ore samples, and higher contents in the upper iron belt than those in the lower belt. The grain size of garnet in the upper iron belt (maximum size reaching up to 15 cm) is much coarser than that in the lower iron belt and middle biotite leptynite (ca. 0.2 ~ 1.0 mm) (Zhou, 1994). The garnet in this study is selected from garnet-chlorite schist which is the altered wall-rock of high-grade iron ore in upper iron ore belt (Fe6, Fig. 4b). The garnet is present as rhombic dodecahedron porphyroblast about 2 cm in size (Fig. 4c). It contains mineral inclusions of magnetite and quartz with developed crack (Fig. 4d), and is surrounded by the matrix mineral

of chlorite (Sun et al., 2014a). It was made a trace element chemical composition profile across the garnet from rim through core to rim, avoiding inclusions and altered minerals.

The migmatitic granite used for zircon U–Pb dating was collected from the upper migmatite zone (Fig. 3). The main mineral assemblage of the gray migmatitic granite is quartz (~40%) + plagioclase (~30%) + K-feldspar (~20%) + muscovite (~10%). The K-feldspar is microcline with across-hatched twinning texture (Fig. 4e, f). Accessory minerals include magnetite, apatite, and zircon. The migmatitic granite is medium–fine grained, and possesses granitic texture.

### 3.2. Analytical methods

#### 3.2.1. Chemical composition of garnet

Trace element including rare earth element (REE) analysis of garnet was conducted by using an Agilent 7700x inductively coupled plasma mass spectrometry (ICP–MS) coupled with an Analyte Excite 193 nm laser at the Laboratory of Mineralization and Dynamics, Chang'an University. In situ sampling on polished-thin sections had been performed by using 32 μm diameter ablation spots with 5 Hz and He as the carrier gas. Element contents were calibrated against multiple reference materials (GSE-1G, BCR-2G, BIR-1G, BHVO-2G, and NIST610). Every six sample analyses were followed by one analysis of NIST610 as quality control to correct the time-dependent drift of sensitivity and mass discrimination. Off-line selection and integration of background and analytic signals, and time drift correction and quantitative calibration were calculated using the program ICPMSDataCal 7.2 (Liu et al., 2010).

#### 3.2.2. Sm–Nd isotopic analysis

Sm–Nd isotopic analysis of garnets was performed at the Analytical Laboratory of the Beijing Research Institute of Uranium Geology, China. The Sm and Nd abundances and $^{143}Nd/^{144}Nd$ ratios were measured on the ISOPROBE-T thermal ionization mass spectrometer. Nd isotopic ratios are normalized to $^{146}Nd/^{144}Nd = 0.7219$ using power law fractionation correction. The Sm and Nd blanks during the course of this study are below $0.5 \times 10^{-10}$. The procedure is described in detail by Wang (1988), Wang et al. (2007). Sm–Nd isochron age was calculated by using the Isoplot 3.0 program (Ludwig, 2003).

#### 3.2.3. Zircon U–Pb isotopic analysis

Zircons were separated from migmatitic granite (15GCL-14) using conventional heavy liquid and magnetic separation techniques. Representative zircon grains were handpicked under a binocular microscope and then were mounted in an epoxy resin disk and polished to about half of their thickness for analysis. Cathodoluminescence (CL) images were obtained in order to reveal the morphology and internal structure of zircons by using a JSM 6510 scanning electron microscope equipped with a Gatan Mono CL System. Zircon U–Pb dating was conducted by using an Agilent 7700× inductively coupled plasma mass spectrometry (ICP–MS) coupled with an Analyte Excite 193 nm laser at the Laboratory of Mineralization and Dynamics, Chang'an University. Zircon 91500 and NIST610 were used as external calibration standards for zircon U–Pb isotope and trace element analyses, respectively. Zircon isotope ratios and trace elements were calculated using the program ICPMSDataCal 7.2 (Liu et al., 2010). Concordia diagrams and weighted mean calculations were carried out using the Isoplot 3.0 program (Ludwig, 2003).

## 4. Results

### 4.1. Garnet trace element composition

The LA–ICP–MS trace element chemical composition profile across the garnet is provided as electronic Supplementary Table A1. The garnet in this study (Sample no. 10GCL-87) is euhedral, and exhibits
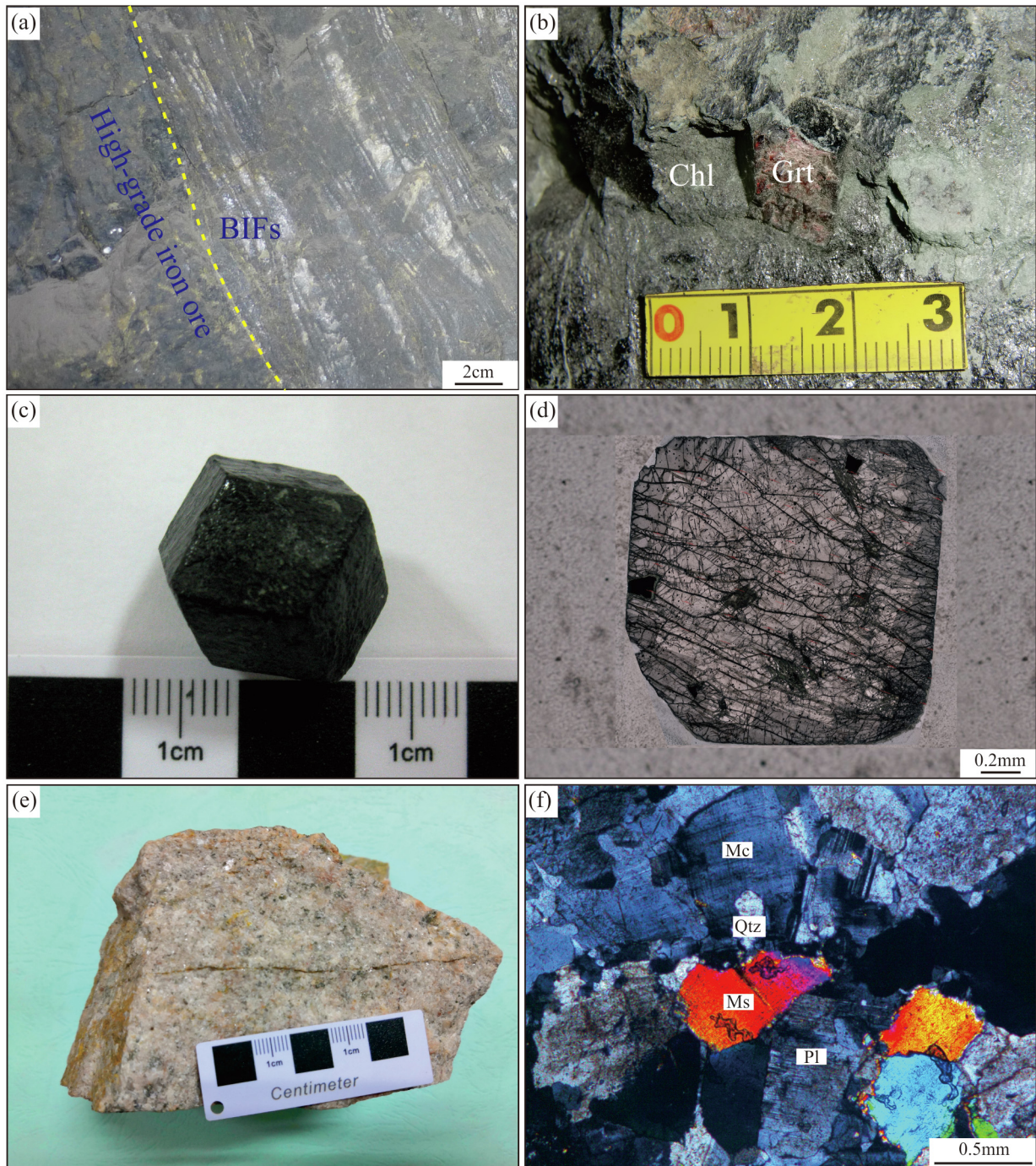
**Fig. 4.** Photos of field, hand specimen and photomicrographs showing the representative mineral assemblage of altered wall-rock, high-grade iron ore and migmatitic granite from the Gongchangling No.2 mining area. (a) Field photo showing the consistent occurrence of BIFs and high-grade in the Fe6 layer; (b) hand specimen of garnet-chlorite schist (10GCL-87) consisting of garnet (Grt) and chlorite (Chl), and the altered schist is wall-rock of a high-grade iron ore in upper iron belt of Fe6; (c) euhedral garnet from garnet-chlorite schist; (d) the developed cracks in garnet (plane-polarized light); (e) hand specimen of gray migmatitic granite; (f) migmatitic granite consisting of quartz (Qtz) + plagioclase (Pl) + K-feldspar + muscovite (Ms), the K-feldspar is microcline (Mc) with across-hatched twinning texture.

pronounced compositional zoning and can be summarized as: (i) MgO and MnO contents exhibit bowl-shaped and shell-shaped patterns, respectively; (ii) Co gradually increases from the core to the rim and (iii) the contents of Ti, V, Li and Sc gradually decrease from the core to the rim (Fig. 5). The Chondrite-normalized REE patterns for all test points show the light REE (LREE) relative to heavy REE (HREE) depletion characteristics, while the middle REE (MREE) relative to HREE changes from depletion in the core to enrichment in the rim (Fig. 6). Moreover, the REE patterns manifest slightly negative or positive (no obvious) Eu

anomalies irregularly without zoning.

### 4.2. Garnet Sm–Nd isochron

Abundances of Sm and Nd of the garnets from five altered wall-rocks of high-grade iron ore and their isotope are listed in Table 1. The concentrations of Sm and Nd are 1.28–2.68 ppm and 1.52–3.63 ppm, respectively. On the $^{147}Sm/^{144}Nd$–$^{143}Nd/^{144}Nd$ diagram, the garnet samples (except for 15GCL-09) display a good linear relationship
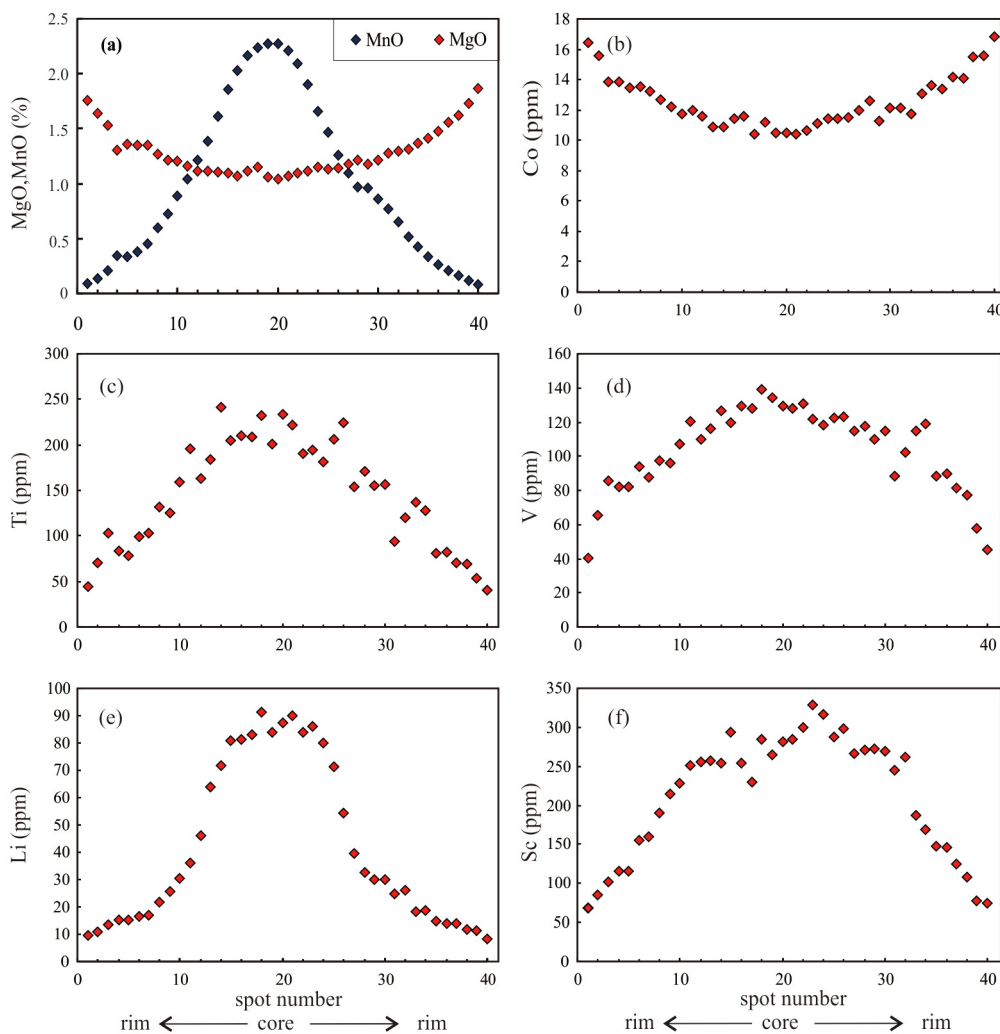
**Fig. 5.** The trace element composition profile of garnet selected from a garnet-chlorite schist (sample no. 10GCL-87).
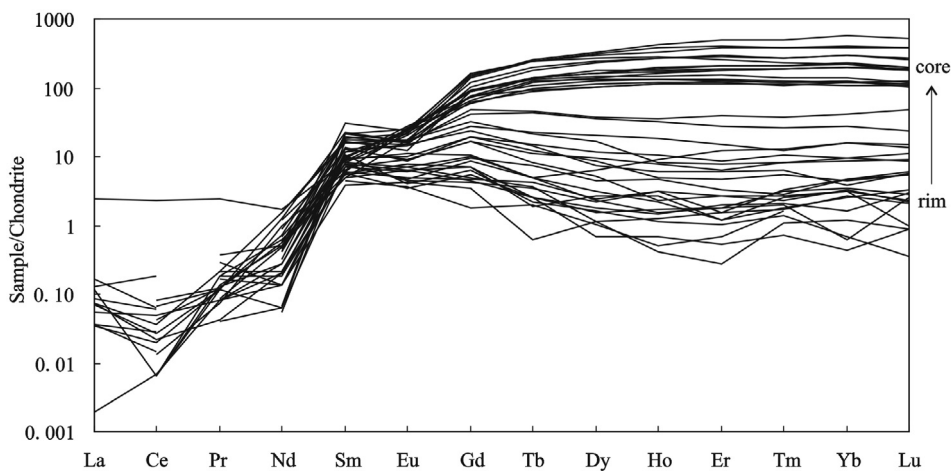


**Fig. 6.** The Chondrite-normalized REE patterns of garnet. The Chondrite values are from Sun and McDonough (1989).

(Fig. 7), which represents an isochron or a mixed line with two end-members of different $^{147}Sm/^{144}Nd$ and $^{143}Nd/^{144}Nd$ ratios (Bell et al., 1989). Because absence of an obvious linear relationship on the $1/Nd$–$^{143}Nd/^{144}Nd$ diagram for the garnets, we can rule out the possibility of a mixed line (Peng et al., 2003; Su et al., 2009). Therefore, the garnets yield a Sm–Nd isochron age of 1888 ± 77 Ma, with a mean

square of weighted deviates (MSWD) of 9.4 and initial $^{143}Nd/^{144}Nd$ ratio of 0.51006 ± 0.00028 ($\varepsilon Nd(t) = -2.6$).

### 4.3. Zircon U–Pb dating

Zircon grains extracted from the migmatitic granite are mainly

**Table 1**

Sm–Nd isotopic composition of garnets from altered wall–rocks of high–grade iron ores in upper iron belt of Fe6 in the Gongchangling iron deposit of the Anshan–Benxi area, NCC.

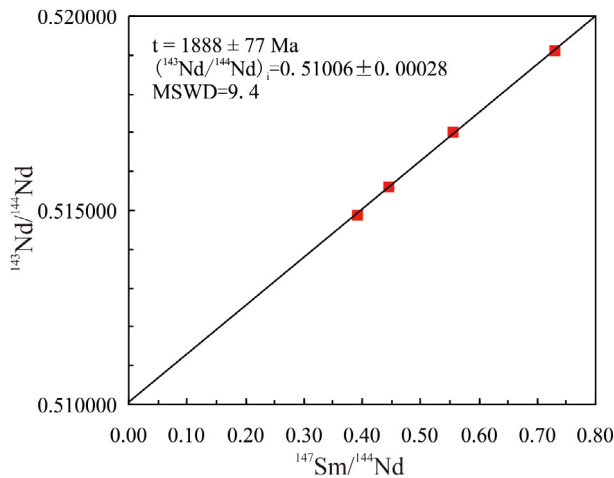| Sample no. | Sm (ppm) | Nd (ppm) | $^{147}Sm/^{144}Nd$ | $^{143}Nd/^{144}Nd$ (2σ) |
|---|---|---|---|---|
| 15GCL-09 | 1.28 | 2.81 | 0.2751 | 0.513002 (14) |
| 15GCL-11 | 1.95 | 2.12 | 0.5567 | 0.517010 (09) |
| 15GCL-12 | 1.84 | 1.52 | 0.7307 | 0.519119 (12) |
| 15GCL-15 | 1.95 | 3.01 | 0.3909 | 0.514897 (12) |
| 10GCL-87 | 2.68 | 3.63 | 0.4453 | 0.515587 (09) |



**Fig. 7.** Sm–Nd isochron for garnets from the altered wall-rocks of high-grade iron ores in the Gongchangling iron deposit of the Anshan-Benxi area, NCC.

stubby or prismatic in shape with a size ranging from 80 to 150 μm. CL images reveal that all zircons are characterized by typical magmatic oscillatory zoning (Hoskin and Schaltegger, 2003; Wu and Zheng, 2004). Fourteen analyses were carried out on fourteen zircons. The results are listed in Table 2 and plotted in the Fig. 8. Nine analyses form a discordant line with an upper intercept age of 2478 ± 36 Ma (MSWD = 2.1), while four analyses of xenocrystic zircon grains closest to concordia define a discordant line with an intercept age of 3105 ± 27 Ma (MSWD = 0.19).
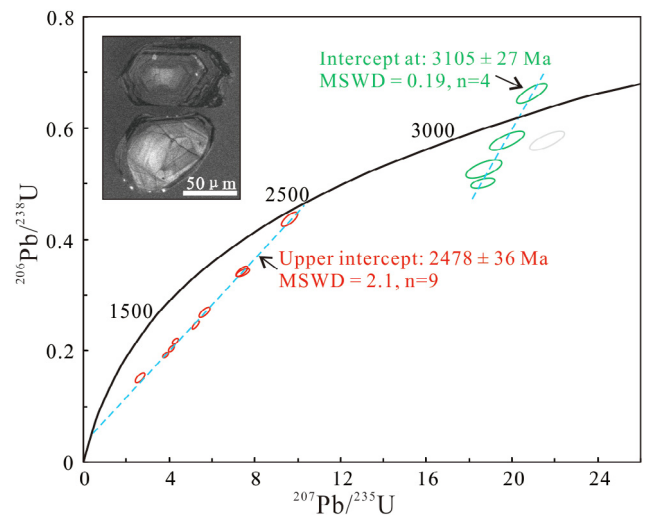


**Fig. 8.** Zircon U–Pb concordia diagram and representative zircon CL image for the migmatitic granite from the Gongchangling iron deposit of the Anshan-Benxi area, NCC.

## 5. Discussion

### 5.1. Age of metamorphism and tectonic affinity

The wall-rock alteration of high-grade iron ore is extensively developed in the Gongchangling No.2 mining area, and the garnet is common in the altered rocks. In general, the proportion of garnet in altered rocks decreases with the increase of the distance from the high-grade iron ore-bodies. Correspondingly, the content of magnetite in altered rock also decreases with the increasing distance from ore-bodies, indicating that the garnet-rich altered rocks and high-grade iron ores have a close not only spatial but also genetic relationship (Li et al., 2014a; Zhu et al., 2016). Since garnets commonly contain unusual amount of minor and trace elements due to substitution, and have chemical zoning, which can provide a continuous physicochemical record of the hydrothermal evolution (Hong et al., 2012; Kotková and Harley, 2010; Rubatto and Hermann, 2007; Vander Auwera and André, 1991; Wang et al., 2002; Zhang et al., 2017).

As mentioned in Section 3.1, the garnet in this study is collected from the altered wall-rock of a high-grade iron ore. Generally, the growth zone of magmatic garnet exhibits specific manganese zoning with a relatively Mn-poor core but a Mn-rich rim, constituting a specific "MnO bowl-shaped profile", due to the gradual increase of Mn/(Fe + Mg) ratios in the cooling crystallization process of magma

**Table 2**

LA–ICP–MS zircon U–Pb isotopic analysis of migmatitic granite from the upper migmatite zone in the Gongchangling iron deposit of the Anshan–Benxi area, NCC.

| Spot | Isotope content (ppm) | | | Ratios | | | | | | Age (Ma) | | | | | |
|---|---|---|---|---|---|---|---|---|---|---|---|---|---|---|---|
| | Th | U | Th/U | $^{207}Pb/^{206}Pb$ | 1σ | $^{207}Pb/^{235}U$ | 1σ | $^{206}Pb/^{238}U$ | 1σ | $^{207}Pb/^{206}Pb$ | 1σ | $^{207}Pb/^{235}U$ | 1σ | $^{206}Pb/^{238}U$ | 1σ |
| 15GCL-14-01 | 150 | 273 | 0.55 | 0.15736 | 0.00370 | 7.39082 | 0.18161 | 0.34069 | 0.00404 | 2427 | 46 | 2160 | 22 | 1890 | 19 |
| 15GCL-14-02 | 525 | 1556 | 0.34 | 0.14455 | 0.00288 | 3.83856 | 0.09958 | 0.19178 | 0.00290 | 2283 | 34 | 1601 | 21 | 1131 | 16 |
| 15GCL-14-03 | 526 | 734 | 0.72 | 0.28122 | 0.00517 | 22.2593 | 0.50688 | 0.57327 | 0.00875 | 3370 | 29 | 3195 | 22 | 2921 | 36 |
| 15GCL-14-04 | 497 | 829 | 0.60 | 0.15574 | 0.00283 | 7.39787 | 0.17716 | 0.34326 | 0.00551 | 2410 | 26 | 2161 | 21 | 1902 | 26 |
| 15GCL-14-05 | 582 | 1422 | 0.41 | 0.14353 | 0.00298 | 4.31238 | 0.09175 | 0.21761 | 0.00283 | 2270 | 35 | 1696 | 18 | 1269 | 15 |
| 15GCL-14-06 | 1623 | 1765 | 0.92 | 0.15495 | 0.00286 | 5.26396 | 0.10974 | 0.24646 | 0.00464 | 2402 | 31 | 1863 | 18 | 1420 | 24 |
| 15GCL-14-07 | 358 | 736 | 0.49 | 0.25411 | 0.00503 | 18.6691 | 0.56181 | 0.52606 | 0.01022 | 3211 | 31 | 3025 | 29 | 2725 | 43 |
| 15GCL-14-08 | 58 | 141 | 0.41 | 0.22836 | 0.00437 | 20.9164 | 0.46584 | 0.66244 | 0.01156 | 3040 | 31 | 3135 | 22 | 3277 | 45 |
| 15GCL-14-09 | 229 | 716 | 0.32 | 0.15950 | 0.00321 | 9.62286 | 0.25447 | 0.43580 | 0.00803 | 2450 | 34 | 2399 | 24 | 2332 | 36 |
| 15GCL-14-10 | 516 | 998 | 0.52 | 0.24621 | 0.00425 | 19.7549 | 0.53851 | 0.57747 | 0.01134 | 3161 | 27 | 3079 | 26 | 2938 | 46 |
| 15GCL-14-11 | 377 | 695 | 0.54 | 0.26894 | 0.00456 | 18.6323 | 0.34553 | 0.50070 | 0.00580 | 3300 | 27 | 3023 | 18 | 2617 | 25 |
| 15GCL-14-12 | 140 | 2115 | 0.07 | 0.12271 | 0.00255 | 2.63370 | 0.13776 | 0.15165 | 0.00600 | 1996 | 37 | 1310 | 39 | 910 | 34 |
| 15GCL-14-13 | 463 | 1375 | 0.34 | 0.15142 | 0.00274 | 5.65364 | 0.15627 | 0.26928 | 0.00558 | 2362 | 31 | 1924 | 24 | 1537 | 28 |
| 15GCL-14-14 | 735 | 1336 | 0.55 | 0.14660 | 0.00301 | 4.10343 | 0.09390 | 0.20340 | 0.00337 | 2306 | 35 | 1655 | 19 | 1194 | 18 |

(Leake, 1967; Miller and Stoddard, 1981; Villaros et al., 2009; Yang et al., 2013). While the bowl-shaped pattern of MgO content and bell-shaped pattern of MnO content are generally interpreted as a growth zoning produced during the prograde metamorphism (Frost and Tracy, 1991; Spear, 1991; Sun et al., 2014; Zhai et al., 1990; Zhang et al., 2000).

The mineral chemical analysis indicates that the garnet is dominated by almandite (Sun et al., 2014a), and records a compositional feature of MgO content with a bowl-shaped profile and MnO content with a bell-shaped profile, indicating it is a metamorphic origin. Moreover, the trace elemental composition of the garnet (Ti, V, Li, Sc and Co) also exhibits a continuous composition zoning (Fig. 5), which suggests that it might be formed during solo geological process.

Redox-sensitive element (U) has different valence states ($U^{4+}$ and $U^{6+}$) and their behaviors are significantly affected by $fO_2$. The $U^{4+}$ is more likely to substitute $Ca^{2+}$ in garnet than $U^{6+}$ (Gaspar et al., 2008; Smith et al., 2004). Therefore, the low contents of U in garnet (0–0.57 ppm, except one spot of 3.68 ppm) indicate that it was formed under relatively high $fO_2$. Since yttrium (Y) and REE show very similar geochemical behavior due to their similar ionic radius and charge (Bau et al., 1996), the garnet records strong positive correlation between REE vs. Y contents (Fig. 9). It is suggested that REE fractionation is dependent strongly on the pH of hydrothermal fluid (Bau, 1991; Zhang et al., 2017). Under mildly acidic conditions, the fluids are commonly LREE-enriched and HREE-depleted with positive Eu anomalies (Bau, 1991), whereas the nearly neutral fluids are HREE-enriched and LREE-depleted with negative or no Eu anomalies (Zhang et al., 2017). The Gongchangling garnet is strongly HREE enriched with no obvious Eu anomalies, suggesting that it was possibly formed in the nearly neutral fluid rather than acidic condition.

Collectively, the Gongchangling garnet was formed during prograde metamorphism, and possibly crystallized from a nearly neutral hydrothermal fluid with relatively high $fO_2$. Therefore, four garnet samples yield the Sm–Nd isochron age of 1888 ± 77 Ma, it is interpreted as time of metamorphism in this area. As the Anshan-Benxi area is adjacent to the Jiao-Liao-Ji Belt, and the Cigou Formation of Anshan Group suffered amphibolite facies metamorphism (Zhai et al., 1990b; Sun et al., 2014a, 2018). It is inferred that the ~1.9 Ga metamorphism in the Gongchangling No.2 mining area was related to the final collision between the Longgang and Langrim Blocks to form the Jiao-Liao-Ji Belt.

### 5.2. Age of migmatization and related tectono-thermal event

There are two types of granitoids in study area, which are located in the hanging-wall and footwall of the Anshan Group supracrustal rock, respectively (Wan, 1994; Li et al., 2015). The age of granitoid in south of the Gongchangling is Mesoarchean (2.99 Ga, Wan, 1994; 3138 ± 6 Ma, Han et al., 2014; 2948 ± 25 Ma, Dong et al., 2017), which is older than the formation age of the Gongchangling BIFs (ca.



**Fig.9.** Diagram of ΣREE vs. Y contents of garnet from sample 10GCL-87.

2.53 Ga, Wan et al., 2012a; Li et al., 2015). Nevertheless, the age of granitoid in north of the Gongchangling is estimated to be ca. 2500 Ma (Wan et al., 2015), which is younger than the formation age of the Gongchangling BIFs.

Zircon U–Pb data from the upper migmatite zone of the Gongchangling No.2 mining area (Mu in Figs. 2, 3) define the intercept ages of 2478 ± 36 Ma and 3105 ± 27 Ma (Fig. 8), respectively. Combined with regional geology in this area, the former, formed at the late Neoarchean–early Paleoproterozoic, is interpreted as the forming age of migmatitic granite, which is roughly contemporaneous with the widespread late Neoarchean granitoids in the Anshan-Benxi area (Wan et al., 2012b, 2015). The latter with age of Mesoarchean, is interpreted as the timing for crystallization age of the protolith of migmatitic granite, due to the extensive exposure of Mesoarchean lithologies in the Anshan-Benxi area (Dong et al., 2017; Long et al., 2019; Wan et al., 2012c).

The Neoarchean is an important continent-formation period with two peaks at ~2.7 Ga and ~2.5 Ga (Condie and Aster, 2010). The tectono-thermal event at ~2.7 Ga widely occurred in many cratons worldwide with global significance, while the ~2.5 Ga tectono-thermal event apparently occurred on a smaller scale and has only been identified in a few cratons. However, the evolution of the NCC is well known for the marked tectono-thermal event at ~2.5 Ga (Dong et al., 2017; Wan et al., 2011, 2012b, c).

Based on the geological and geochronological data, three ancient terranes (> 2.6 Ga) are identified, namely the eastern, southern and central ancient terranes, and these terranes define a foundation for the late Neoarchean tectonic evolution of the NCC (Wan et al., 2015, 2018). During the late Neoarchean, the plate tectonic system already played a role in the NCC, and three ancient terranes were located in the ocean and amalgamated together by subductions and collisions. In the late Neoarchean, these terranes entered the extension stage, which further led to the primary cratonization of the NCC. The Anshan-Benxi area is located in the northern part of the eastern ancient terrane at that time. The BIFs in the Anshan-Benxi area are main Algoma-type with age of 2.52–2.55 Ga (Wan et al., 2012a, 2016; Sun et al., 2014b; Tong et al., 2019; Zhang et al., 2012, 2016), indicating a relatively stable environment at that time (Wan et al., 2015). The ca. 2.5 Ga granitoids which are slightly younger than BIFs, were probably formed in an extensional tectonic setting, resulting from the underplating of mantle derived magmas (Wan et al., 2012a,b,c; Zhao et al., 1998).

The Gongchangling migmatitic granite in the Anshan-Benxi area of the NCC was formed at ca. 2.5 Ga, inferred that it might be related to the ~2.5 Ga tectono-thermal event in the NCC.

### 5.3. Genesis of high-grade iron ore

As to the genesis of the high-grade iron ore in the Gongchangling No.2 mining area, there are three different opinions for a long time, including: (1) the high-grade iron ore was mainly formed during original deposition stage, and subsequently modified by diagenesis (Chen et al., 1984); (2) it was formed during hydrothermal reformation stage. The silica of BIFs was leached out by the hydrothermal fluid, while the magnetite of BIFs was reserved forming the high-grade iron ore. However, the nature of the hydrothermal fluid is debated within migmatitic hydrothermal fluid, metamorphic hydrothermal fluid and meteoric fluid (Li et al., 2015; Liu and Jin, 2010; Wang et al., 2012; and references therein); (3) the graphite-bearing high-grade iron ore was formed by decomposition of siderite during metamorphism (Li, 1982; Li et al., 1983).

The high-grade iron ores mainly occurred within BIFs, and show obvious structure-controlled (faults and folds) characteristics (Zhou, 1994). The intensity of wall-rock alteration is roughly proportional to the scale of high-grade iron ores (Wang et al., 2014; Zhu et al., 2016). All these evidences indicate that the genesis of the Gongchangling high-grade iron ore is related with the hydrothermal enrichment (Sun et al.,
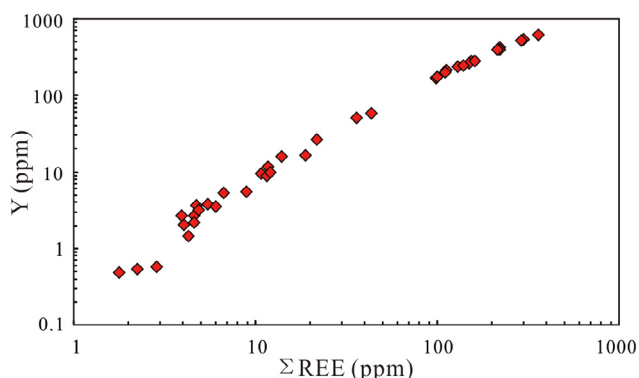
**Table 3**
Age comparison for ore and related rocks in the Gongchangling iron deposit of the Anshan-Benxi area, NCC.

| Items | Testing object | Analytical method | Age | Reference |
|---|---|---|---|---|
| BIFs | Leptynite (Fine grained biotite-plagioclase gneiss), interlayer of BIFs | Zircon SHRIMP | 2528 ± 10 Ma | Wan et al., 2012a,b,c |
| | Leptynite (Fine grained biotite-plagioclase gneiss), interlayer of BIFs | Zircon SHRIMP | 2539 ± 25 Ma | Li et al, 2016 |
| | Plagioclase-hornblende schist, wall-rock of BIFs | Zircon SHRIMP | 2554 ± 12 Ma | Han et al., 2014 |
| High-grade iron ore | Garnet-rich altered rock | Zircon SHRIMP | 1840 ± 7 Ma | Li et al., 2014a,b |
| | Garnet-rich altered rock | Monazite and zircon SHRIMP | 1860 ± 7 Ma | Li et al, 2019 |
| Metamorphism | Garnet-chlorite schist, wall-rock of high-grade iron ore | Garnet Sm-Nd isochron | 1888 ± 77 Ma | This study |
| Migmatization | Migmatitic granite | Zircon LA-ICP-MS | 2478 ± 36 Ma | This study |
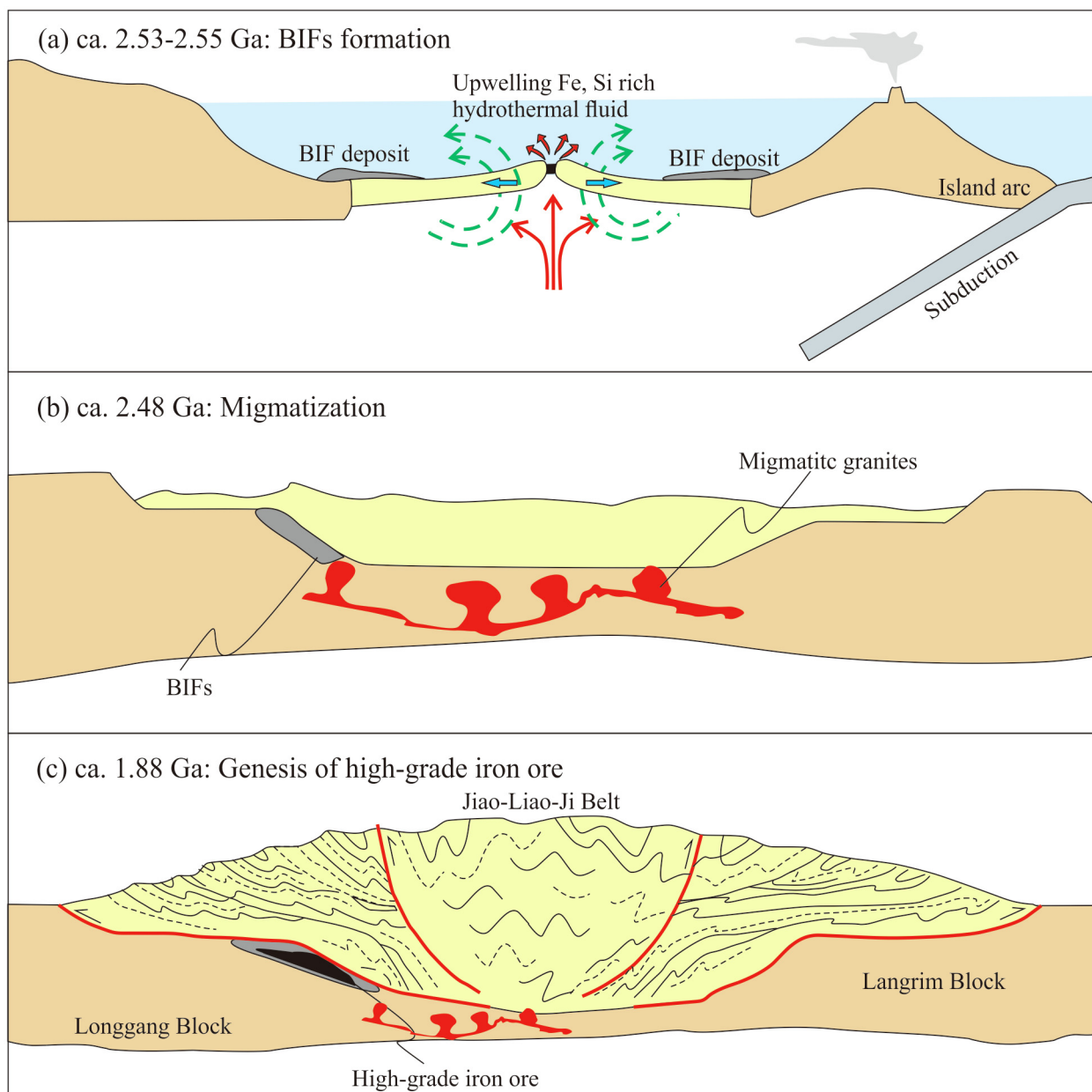


Fig. 10. Schematic diagram showing the genesis of the Gongchangling BIF-related high-grade iron ore.

2014a, 2018; Wang et al., 2014; Li et al., 2015). The biotite leptynite interlayer in the Gongchangling BIFs constrained the formation age of the BIFs at late Neoarchean (2528 ± 10 Ma, Wan et al., 2012a; 2554 ± 12 Ma, Han et al., 2014; 2539 ± 25 Ma, Li et al., 2016). Hydrothermal zircon and monazite from the altered wall-rock of the high-grade iron ores indicated that the age of the high-grade iron ores was late Paleoproterozoic (1840 ± 7 Ma, Li et al., 2014a;

1860 ± 7 Ma, Li et al., 2019). Since the meteoric fluids were acidic in the Paleoproterozoic, furthermore, when it passed through the carbonate of Liaohe Group into the Gongchangling BIFs, it would become more acidic (Chen, 2000; Li et al., 2014c). However, the REE pattern for the Gongchangling garnet indicates that it was formed in the nearly neutral fluid. In addition, the altered wall-rocks near high-grade iron ore-bodies suggests that the hydrothermal alteration in the

Gongchangling occurred under neutral–alkaline condition (Li et al., 2015). Therefore, the influence of meteoric fluid on the formation of high-grade iron ore was relatively limited.

In this study, we obtained the ages of the metamorphism (1888 ± 77 Ma) and migmatization (2478 ± 36 Ma). Compared with these ages (Table 3), it shows that the forming age of high-grade iron ores is contemporary with the time of metamorphism rather than migmatization, indicating that the genesis of the high-grade iron ores was related with the enrichment of BIFs by metamorphic hydrothermal fluids.

The genesis of the high-grade iron ore related with metamorphic hydrothermal fluid, can also be supported by other evidences as follows: (1) the BIFs and high-grade iron ores show similar whole-rock geochemical characteristics indicating that the hydrothermal fluids were from ore itself with little addition of foreign materials (Liu and Jin, 2010; Sun et al., 2014a; Zhou, 1994); (2) the sulfur and oxygen isotopes characteristics exclude the migmatitic hydrothermal fluid to form the high-grade iron ores (Liu and Jin, 2010; Wang et al., 2012); (3) the fluid inclusion characteristics of high-grade iron ores are similar to those of BIFs, but show obvious differences with those of the migmatitic granite (Shi and Li, 1980).

Combined with previous studies, the process for genesis of the high-grade iron ores in the Gongchangling No.2 mining area can be summarized as follows (Fig. 10): (1) at the late Neoarchean (ca. 2.53–2.55 Ga), the Gongchangling BIFs were formed in an active tectonic setting and the ore-forming material of Fe and Si sourced from the submarine hydrothermal fluid; (2) after a short time interval, the ca. 2.5 Ga tectono-thermal event resulted in formation of the migmatitic granites, steeply dipping BIFs-bearing sequences and recrystallization of magnetite (Li et al., 2019); (3) at the late Paleoproterozoic Orosirian (ca. 1.88 Ga), the Cigou Formation of the Anshan Group suffered lower amphibolite facies metamorphism due to the formation of Jiao-Liao-Ji Belt. The metamorphic hydrothermal fluids flowed through BIFs along the weak tectonic zone would dissolve silica to enrich the ore, as a result, the reformed BIFs became high-grade iron ores.

## 6. Conclusion

(1) The trace elemental composition of a garnet from an altered wall-rock of high-grade iron ore indicates that the garnet was formed under neutral condition with a metamorphic origin. A Sm–Nd isochron age of 1888 ± 77 Ma dated by the garnets, is interpreted as the age of metamorphism.

(2) LA–ICP–MS U–Pb dating of zircons from upper migmatite zone shows that the migmatitic granite was formed at 2478 ± 36 Ma, which was related to the ~2.5 Ga tectono-thermal event in the NCC.

(3) Combined with previous studies and compared the ages of metamorphism and migmatization with high-grade iron ores, it is indicated that the high-grade iron ores in the Gongchangling iron deposit are the reformed products of BIFs by the metamorphic hydrothermal fluids.

## Declaration of Competing Interest

The authors declare that they have no known competing financial interests or personal relationships that could have appeared to influence the work reported in this paper.

## Acknowledgements

## Appendix A. Supplementary data

Supplementary data to this article can be found online at https://doi.org/10.1016/j.oregeorev.2020.103504.

## References

Bai, J., 1993. The Precambrian Geology and Pb–Zn Mineralization in the Northern Margin of North China Platform. Geological Publishing House, Beijing, pp. 47–89 (in Chinese).

Bau, M., 1991. Rare–earth element mobility during hydrothermal and metamorphic fluid-rock interaction and the significance of the oxidation state of europium. Chem. Geol. 93, 219–230.

Bau, M., Koschinsky, A., Dulski, P., Hein, J., 1996. Comparison of the partitioning behaviours of yttrium, rare earth elements, and titanium between hydrogenetic marine ferromanganese crusts and seawater. Geochim. Cosmochim. Acta 60, 1709–1725.

Bekker, A., Slack, J.F., Planavsky, N., Krapež, B., Hofmann, A., Konhauser, K.O., Rouxel, O.J., 2010. Iron formation: the sedimentary product of a complex interplay among mantle, tectonic, oceanic, and biospheric processes. Econ. Geol. 105, 467–508.

Bell, K., Anglin, C., Franklin, J., 1989. Sm–Nd and Rb–Sr isotope systematics of scheelites: possible implications for the age and genesis of vein–hosted gold deposits. Geology 17, 500–504.

Chen, F., 2000. Constraints of atmosphere and seawater evolution on the origin and progress of animals. Geol.–Geochem. 28 (2), 67–75 (in Chinese with English abstract).

Chen, Y.J., Ouyang, Z.Y., Yang, Q.J., Deng, J., 1994. A new understanding of the Archean-Proterozoic boundary. Geol. Rev. 40, 483–488 (in Chinese with English abstract).

Chen, G.Y., Sun, D.S., Sun, C.M., Li, M.H., Wang, X.F., Wang, Z.F., 1984. Genesis of Gongchangling iron deposit. J. Mineral. Petrol. 4, 1–266 (in Chinese).

Chen, J.F., Yang, Y.L., Li, P., Cheng, W.J., Zhou, T.X., Liu, Y.P., 1985. Sulfur isotope study on the genesis of high-grade iron deposit in Anshan-Benxi area, Liaoning Province. Geol. Prospect. 21, 32–37 (in Chinese).

Chen, Y.J., Zhao, Y.C., 1997. Geochemical characteristics and evolution of REE in the Early Precambrian sediments: evidences from the southern margin of the North China Craton. Episodes 20, 109–116.

Cheng, Y.Q., 1957. Problems on the high-grade ore in the Presinian (Precambrian) banded iron ore deposits of the Anshan type of Liaoning and Shandong Provinces. Acta Geol. Sin. 33, 153–180 (in Chinese with English abstract).

Chi, W.Z., 1993. Second mining area of Gongchangling iron deposit, in: Chinese iron ore deposit. Metallurgical Industry Press, Beijing, pp. 279–284 (in Chinese).

Clout, J., 2006. Iron formation–hosted iron ores in the Hamersley Province of Western Australia. Appl. Earth Sci. 115, 115–125.

Condie, K.C., Aster, R.C., 2010. Episodic zircon age spectra of orogenic granitoids: the supercontinent connection and continental growth. Precambr. Res. 180, 227–236.

Cui, P.L., Sun, J.G., Sha, D.M., Wang, X.J., Zhang, P., Gu, A.L., Wang, Z.Y., 2013. Oldest zircon xenocryst (4.17 Ga) from the North China Craton. Int. Geol. Rev. 55, 1902–1908.

Dai, Y.P., Zhang, L.C., Zhu, M.T., Wang, C.L., Liu, L., Xiang, P., 2014. The composition and genesis of the Mesoarchean Dagushan banded iron formation (BIF) in the Anshan area of the North China Craton. Ore Geol. Rev. 63, 353–373.

Dong, C., Wan, Y., Xie, H., Nutman, A.P., Xie, S., Liu, S., Ma, M., Liu, D., 2017. The Mesoarchean Tiejiashan-Gongchangling potassic granite in the Anshan-Benxi area, North China Craton: origin by recycling of Paleo– to Eoarchean crust from U-Pb–Nd–Hf–O isotopic studies. Lithos 290–291, 116–135.

Egglseder, M.S., Cruden, A.R., Dalstra, H.J., Nicholas, L., 2017. The role of deformation in the formation of banded iron formation–hosted high-grade iron ore deposits, Hamersley Province (Australia). Precambr. Res. 296, 62–77.

Faure, M., Lin, W., Monie, P., Bruguier, O., 2004. Palaeoproterozoic arc magmatism and collision in Liaodong Peninsula (north–east China). Terra Nova 16, 75–80.

Figueiredo e Silva, R.C., Hagemann, S., Lobato, L.M., Rosière, C.A., Banks, D.A., Davidson, G.J., Vennemann, T., Hergt, J., 2013. Hydrothermal fluid processes and evolution of the giant Serra Norte jaspilite–hosted iron ore deposits, Carajás Mineral Province, Brazil. Econ. Geol. 108, 739–779.

Frost, B.R., Tracy, R.J., 1991. PT paths from zoned garnets: some minimum criteria. Am. J. Sci. 291, 917–939.

Gaspar, M., Knaack, C., Meinert, L., Moretti, R., 2008. REE in skarn systems: A LA–ICP–MS study of garnets from the Crown Jewel gold deposit. Geochim. Cosmochim. Acta 72, 185–205.

Gross, G.A., 1980. A classification of iron–formation based on depositional environments. Can. Mineral. 18, 215–222.

Guan, G.Y., 1961. The significance of metemorphism in the genesis of high-grade iron ore. Acta Geol. Sin. 41, 65–76 (in Chinese with Russian abstract).

Hagemann, S.G., Angerer, T., Duuring, P., Rosière, C.A., Figueiredo e Silva, R.C., Lobato, L., Hensler, A.S., Walde, D.H.G., 2016. BIF–hosted iron mineral system: A review. Ore Geol. Rev. 76, 317–359.

Han, C.M., Xiao, W.J., Su, B.X., Sakyi, P.A., Chen, Z.L., Zhang, X.H., Ao, S.J., Zhang, J.,

Wan, B., Zhang, Z.Y., Wang, Z.M., Ding, J.X., 2014. Formation age and genesis of the Gongchangling Neoarchean banded iron deposit in eastern Liaoning Province: constraints from geochemistry and SHRIMP zircon U-Pb dating. Precambr. Res. 254, 306–322.

Hong, W., Zhang, Z.H., Jiang, Z.S., Li, F.M., Liu, X.Z., 2012. Magnetite and garnet trace element characteristics from the Chagangnuoer iron deposit in the western Tianshan Mountains, Xinjiang, NW China: constrain for ore genesis. Acta Petrol. Sin. 28 (7), 2089–2102 (in Chinese with English abstract).

Hoskin, P.W., Schaltegger, U., 2003. The composition of zircon and igneous and metamorphic petrogenesis. Rev. Mineral. Geochem. 53, 27–62.

Hou, K.J., Ma, X.D., Li, Y.H., Liu, F., Han, D., 2019. Genesis of Huoqiu banded iron formation (BIF), southeastern North China Craton, constraints from geochemical and Hf–O–S isotopic characteristics. J. Geochem. Explor. 197, 60–69.

Huston, D.L., Logan, G.A., 2004. Barite, BIFs and bugs: evidence for the evolution of the Earth's early hydrosphere. Earth Planet. Sci. Lett. 220, 41–55.

James, H.L., 1954. Sedimentary facies of iron–formation. Econ. Geol. 49, 235–293.

Klein, C., 2005. Some Precambrian banded iron–formations (BIFs) from around the world: their age, geologic setting, mineralogy, metamorphism, geochemistry, and origin. Am. Mineral. 90, 1473–1499.

Konhauser, K.O., Pecoits, E., Lalonde, S.V., Papineau, D., Nisbet, E.G., Barley, M.E., Arndt, N.T., Zahnle, K., Kamber, B.S., 2009. Oceanic nickel depletion and a methanogen famine before the Great Oxidation Event. Nature 458, 750–754.

Konhauser, K.O., Planavsky, N.J., Hardisty, D.S., Robbins, L.J., Warchola, T.J., Haugaard, R., Lalonde, S.V., Partin, C.A., Oonk, P.B.H., Tsikos, H., Lyons, T.W., Bekker, A., Johnson, C.M., 2017. Iron formations: a global record of Neoarchaean to Palaeoproterozoic environmental history. Earth Sci. Rev. 172, 140–177.

Kotková, J., Harley, S., 2010. Anatexis during high–pressure crustal metamorphism: evidence from garnet–whole–rock REE relationships and zircon–rutile Ti–Zr thermometry in leucogranulites from the Bohemian Massif. J. Petrol. 51, 1967–2001.

Lascelles, D., 2012. Banded iron formation to high-grade iron ore: a critical review of supergene enrichment models. Aust. J. Earth Sci. 59, 1105–1125.

Leake, B.E., 1967. Zoned garnets from the galway granite and its aplites. Earth Planet. Sci. Lett. 3, 311–316.

Li, S.G., 1982. Geochemical model for the genesis of the Gongchangling rich magnetite deposit in China. Geochimica 11, 113–121 (in Chinese with English abstract).

Li, Z., Chen, B., Wei, C.J., 2017. Is the Paleoproterozoic Jiao–Liao–Ji Belt Belt (North China Craton) a rift? Int. J. Earth Sci. 106, 355–375.

Li, B.L., Li, X.M., Cui, X.F., Wang, Z.L., 1977. Fluid inclusions thermometry of mineral from Gongchangling No.2 mining area. J. Univ. Sci. Tech. China 7, 96–103 (in Chinese).

Li, L.X., Li, H.M., Liu, M.J., Yang, X.Q., Meng, J., 2016. Timing of deposition and tectonothermal events of banded iron formations in the Anshan-Benxi area, Liaoning Province, China: evidence from SHRIMP U-Pb zircon geochronology of the wall rocks. J. Asian Earth Sci. 129, 276–293.

Li, H.M., Liu, M.J., Li, L.X., Yang, X.Q., Yang, L.D., Chen, J., Yao, T., 2014a. SHRIMP U-Pb geochronology of zircons from the garnet–rich altered rocks in the mining area II of the Gongchangling iron deposit: constraints on the ages of the high-grade iron deposit. Acta Petrol. Sin. 30 (5), 1205–1217 (in Chinese with English abstract).

Li, H.M., Yang, X.Q., Li, L.X., Zhang, Z.C., Liu, M.J., Yao, T., Chen, J., 2015. Desilicification and iron activation–reprecipitation in the high-grade magnetite ores in BIFs of the Anshan-Benxi area, China: evidence from geology, geochemistry and stable isotopic characteristics. J. Asian Earth Sci. 113, 998–1016.

Li, Y.H., Zhang, Z.J., Hou, K.J., Duan, C., Wan, D.F., Hu, G.Y., 2014c. The genesis of Gongchangling high-grade iron ores, Anshan-Benxi area, Liaoning province, NE China: evidence from Fe-Si-O-S isotopes. Acta Geol. Sin. 88, 2351–2372 (in Chinese with English abstract).

Li, H.M., Zhang, Z.J., Li, L.X., Zhang, Z.C., Chen, J., Yao, T., 2014b. Types and general characteristics of the BIF–related iron deposits in China. Ore Geol. Rev. 57, 264–287.

Li, S.Z., Zhao, G.C., 2007. SHRIMP U-Pb zircon geochronology of the Liaoji granitoids: constraints on the evolution of the Paleoproterozoic Jiao–Liao–Ji belt in the Eastern Block of the North China Craton. Precambr. Res. 158, 1–16.

Li, S.G., Zhi, C.X., Chen, J.F., Wang, J.X., Deng, Y.Y., 1983. Origin of graphites in early Precambrian banded iron formation in Anshan, China. Geochimica 12, 162–169 (in Chinese with English abstract).

Li, L.X., Zi, J.W., Li, H.M., Rasmussen, B., Wilde, S.A., Sheppard, S., Ma, Y.B., Meng, J., Song, Z., 2019. High-grade magnetite mineralization at 1.86 Ga in neoarchean banded iron formations, Gongchangling, China. in situ U-Pb geochronology of metamorphic-hydrothermal zircon and monazite. Econ. Geol. 114, 1159–1175.

Liu, Y.S., Hu, Z.C., Zong, K.Q., Gao, C.G., Shan, G., 2010. Reappraisal and refinement of zircon U-Pb isotope and trace element analyses by LA–ICP–MS. Sci. Bull. 55, 1535–1546.

Liu, J., Jin, S.Y., 2010. Genesis study of magnetite–rich ore in Gongchangling iron deposit, Liaoning. Geoscience 24, 80–88 (in Chinese with English abstract).

Liu, J., Zhang, J., Liu, Z., Yin, C., Zhao, C., Li, Z., Yang, Z., Dou, S., 2018. Geochemical and geochronological study on the Paleoproterozoic rock assemblage of the Xiuyan region: new constraints on an integrated rift–and–collision tectonic process involving the evolution of the Jiao–Liao–Ji Belt, North China Craton. Precambr. Res. 310, 179–197.

Long, X.P., Yang, W., Lin, Y.T., Yang, J.H., Hao, J.L., Zhang, J.C., 2019. Sub-micron trace elemental distributions and U-Pb dating of zircon from the oldest rock in the Anshan area, North China Craton. Precambr. Res. 322, 1–17.

Ludwig, K.R., 2003. ISOPLOT 3.0: A geochronological toolkit for Microsoft excel. Berkeley Geochronology Center, Berkeley.

Miller, C., Stoddard, E., 1981. The Role of Manganese in the Paragenesis of Magmatic Garnet: an example from the old woman-piute range, California. J. Geol. 89, 233–246.

Moon, I., Lee, I., Yang, X., 2017. Geochemical constraints on the genesis of the Algoma–type banded iron formation (BIF) in Yishui County, western Shandong Province, North China Craton. Ore Geol. Rev. 89, 931–945.

Peng, J.T., Hu, R.Z., Burnard, P.G., 2003. Samarium–neodymium isotope systematics of hydrothermal calcites from the Xikuangshan antimony deposit (Hunan, China): the potential of calcite as a geochronometer. Chem. Geol. 200, 129–136.

Peng, Q.M., Palmer, M.R., 1995. The Paleoproterozoic boron deposits in eastern Liaoning, China: a metamorphosed evaporate. Precambr. Res. 72, 185–197.

Rubatto, D., Hermann, J., 2007. Experimental zircon/melt and zircon/garnet trace element partitioning and implications for the geochronology of crustal rocks. Chem. Geol. 241, 38–61.

Shi, J.X., Li, B.C., 1980. Origin of rich magnetite ores in the Gongchangling area as evidenced by fluid inclusion studies from the Anshan-Benxi region, Northeast China. Geochimica 9, 43–53 (in Chinese with English abstract).

Smith, M., Henderson, P., Jeffries, T., Long, J., Williams, C.T., 2004. The rare earth elements and uranium in garnets from the Beinn an Dubhaich Aureole, Skye, Scotland, UK: constraints on processes in a dynamic hydrothermal system. J. Petrol. 45, 457–484.

Song, B., Nutman, A.P., Liu, D.Y., Wu, J.S., 1996. 3800 to 2500 Ma crustal evolution in the Anshan area of Liaoning Province, northeastern China. Precambr. Res. 78, 79–94.

Spear, F., 1991. On the interpretation of peak metamorphic temperatures in light of garnetdiffusion during cooling. J. Metamorph. Geol. 9, 379–388.

Spier, C.A., de Oliveira, S.M.B., Rosière, C.A., Ardisson, J.D., 2008. Mineralogy and trace–element geochemistry of the high-grade iron ores of the Águas Claras Mine and comparison with the Capão Xavier and Tamanduá iron ore deposits, Quadrilátero Ferrífero, Brazil. Miner. Deposita 43, 229–254.

Su, W.C., Hu, R.Z., Xia, B., Xia, Y., Liu, Y.P., 2009. Calcite Sm–Nd isochron age of the Shuiyindong Carlin–type gold deposit, Guizhou, China. Chem. Geol. 258, 269–274.

Sun, S.S., McDonough, W.F., 1989. Chemical and isotopic systematics of oceanic basalts: implications for mantle composition and processes. In: Saunders, A. D. and Norry, M. J. (Eds.), Magmatism in the Ocean basins. Geological Society of London Special Publication 42, 313–345.

Sun, X.H., Zhu, X.Q., Tang, H.S., Zhang, Q., Luo, T.Y., Han, T., 2014b. Protolith reconstruction and geochemical study on the wall rocks of Anshan BIFs, Northeast China: implications for the provenance and tectonic setting. J. Geochem. Explor. 136, 65–75.

Sun, X.H., Zhu, X.Q., Tang, H.S., Zhang, Q., Luo, T.Y., 2014a. The Gongchangling BIFs from the Anshan-Benxi area, NE China: petrological–geochemical characteristics and genesis of high-grade iron ores. Ore Geol. Rev. 60, 112–125.

Sun, X.H., Zhu, X.Q., Tang, H.S., Luan, Y., 2018. In situ LA–ICP–MS trace element analysis of magnetite from the late Neoarchean Gongchangling BIFs, NE China: constraints on the genesis of high-grade iron ore. Geol. J. 53 (S1), 8–20.

Tang, H.S., Chen, Y.J., Santosh, M., Zhong, H., Yang, T., 2013b. REE geochemistry of carbonates from the Guanmenshan Formation, Liaohe Group, NE Sino-Korean Craton: implications for seawater compositional change during the Great Oxidation Event. Precambr. Res. 227, 316–336.

Tang, H.S., Chen, Y.J., Santosh, M., Zhong, H., Wu, G., Lai, Y., 2013a. C-O isotope geochemistry of the Dashiqiao magnesite belt, North China Craton: implications for the Great Oxidation Event and ore genesis. Geol. J. 48, 467–483.

Thorne, W., Hagemann, S., Vennemann, T., Oliver, N., 2009. Oxygen isotope compositions of iron oxides from high-grade BIF–hosted iron ore deposits of the Central Hamersley Province, Western Australia: constraints on the evolution of hydrothermal fluids. Econ. Geol. 104, 1019–1035.

Tong, X.X., Wang, C.L., Peng, Z.D., Huang, H., Zhang, L.C., Zhai, M.G., 2019. Geochemistry of meta–sedimentary rocks associated with the Neoarchean Dagushan BIF in the Anshan-Benxi area, North China Craton: implications for their provenance and tectonic setting. Precambr. Res. 325, 172–191.

Vander Auwera, J., André, L., 1991. Trace elements (REE) and isotopes (O, C, Sr) to characterize the metasomatic fluid sources: evidence from the skarn deposit (Fe, W, Cu) of Traversella (Ivrea, Italy). Contrib. Mineral. Petr. 106, 325–339.

Villaros, A., Stevens, G., Buick, I.S., 2009. Tracking S–type granite from source to emplacement: clues from garnet in the Cape Granite Suite. Lithos 112, 217–235.

Wan, Y.S., 1994. Formation and Evolution o the Iron–Bearing Rock Series of Gongchangling area, Liaoning Province. Beijing Science and Technology Press, Beijing 108 p (in Chinese).

Wan, Y.S., Liu, D.Y., Wang, S.J., Yang, E.X., Wang, W., Dong, C.Y., Zhou, H.Y., Du, L.L., Yang, Y.H., Diwu, C.R., 2011. ~2.7 Ga juvenile crust formation in the North China Craton (Taishan–Xintai area, western Shandong Province): further evidence of an understated eent from U-Pb dating and Hf isotopic composition of zircon. Precambr. Res. 186, 169–180.

Wan, Y.S., Dong, C.Y., Xie, H.Q., Wang, S.J., Song, M.C., Xu, Z.Y., Wang, S.Y., Zhou, H.Y., Ma, M.Z., Liu, D.Y., 2012a. Formation ages of early Precambrian BIFs in the North China Craton: SHRIMP zircon U-Pb dating. Acta Geol. Sin. 86, 1447–1478 (in Chinese with English abstract).

Wan, Y.S., Liu, D.Y., Nutman, A., Zhou, H.Y., Dong, C.Y., Yin, X.Y., Ma, M.Z., 2012c. Multiple 3.8–3.1Ga tectono–magmatic events in a newly discovered area of ancient rocks (the Shengousi Complex), Anshan, North China Craton. J. Asian Earth Sci. 54–55, 18–30.

Wan, Y.S., Dong, C., Liu, D., Kröner, A., Yang, C., Wang, W., Du, L., Xie, H., Ma, M., 2012b. Zircon ages and geochemistry of late Neoarchean syenogranites in the North China Craton: a review. Precambrian Res. 222–223, 265–289.

Wan, Y.S., Ma, M.Z., Dong, C.Y., Xie, H.Q., Xie, S.W., Ren, P., Liu, D.Y., 2015. Widespread late Neoarchean reworking of Meso- to Paleoarchean continental crust in the Anshan-Benxi area, North China Craton, as documented by U-Pb–Nd–Hf–O isotopes. Am. J. Sci. 315, 620–670.

Wan, Y.S., Liu, D.Y., Xie, H.Q., Kröner, A., Ren, P., Liu, S.J., Xie, S.W., Dong, C.Y., Ma,

M.Z., 2016. Neoarchean Banded Iron Formations in the North China Craton: geology, geochemistry, and its implications. In: Zhai, M.G. (Ed.), Main Tectonic Events and Metallogeny of the North China Craton. Springer, pp. 65–83.

Wan, Y.S., Liu, S.J., Xie, H.Q., Dong, C.Y., Li, Y., Bai, W.Q., Liu, D.Y., 2018. Formation and evolution of the Archean continental crust of China: a review. Chin. Geol. 1, 109–136.

Wang, Y.X., 1988. A study of the Sm–Nd method for fossil mineral and rock and its applications. J. Nanjing Univ. 24 (2), 297–308 (in Chinese with English abstract).

Wang, L. J., Wang, J. B., Wang, Y. W., Hidehiko, S., 2002. REE geochemistry, of the Huangguangliang skarn Fe–Sn deposit, inner Mongolia. Acta Petrol. Sin. 2002, 18(4), 575–584 (in Chinese with English abstract).

Wang, F., Liu, F.L., Liu, P.H., Cai, J., Schertl, H.P., Ji, L., Liu, L.S., Tian, Z.H., 2017. In situ zircon U-Pb dating and whole–rock geochemistry of metasedimentary rocks from South Liaohe Group, Jiao–Liao–Ji orogenic belt: constraints on the depositional and metamorphic ages, and implications for tectonic setting. Precambr. Res. 303, 764–780.

Wang, E.D., Xia, J.M., Zhao, C.F., Fu, J.F., Hou, B.G., 2012. Forming mechanism of high-grade magnetite bodies in Gongchangling, Liaoning. Acta Geol. Sin. 86, 1761–1772 (in Chinese with English abstract).

Wang, E.D., Xia, J.M., Zhao, C.F., Fu, J.F., Hou, B.G., 2013. Material source and sedimentary environment of Gongchangling iron deposit. Miner. Deposits 32, 380–396 (in Chinese with English abstract).

Wang, E.D., Xia, J.M., Fu, J.F., Jia, S.S., Men, Y.K., 2014. Formation mechanism of Gongchangling high-grade magnetite deposit hosted in Archean BIF, Anshan-Benxi area, Northeastern China. Ore Geol. Rev. 57, 308–321.

Wang, Y.X., Yang, J.D., Chen, J., Zhang, K.J., Rao, W.B., 2007. The Sr and Nd isotopic variations of the Chinese Loess Plateau during the past 7 Ma: implications for the East Asian winter monsoon and source areas of loess. Palaeogeogr. Palaeoclimatol. Palaeoecol. 249 (3–4), 351–361.

Wu, Y.B., Zheng, Y.F., 2004. Genesis of zircon and its constraints on interpretation of U-Pb age. Chin. Sci. Bull. 49, 1554–1569 (in Chinese).

Xu, Z.H., Sun, F.Y., Xin, W., Sun, N.R., Li, F.W., Niu, J.P., Li, L., Li, G.X., 2019. Formation and evolution of Paleoproterozoic orogenic belt in southern Jilin, Jiao–Liao–Ji Belt, North China Craton: constraints from geophysics. Precambr. Res. 333, 105433.

Yang, J.H., Peng, J.T., Hu, R.Z., Bi, X.W., Zhao, J.H., Fu, Y.Z., Shen, N.P., 2013. Garnet geochemistry of tungsten-mineralized Xihuashan granites in South China. Lithos 177, 79–90.

Yang, X.Q., Zhang, Z.H., Duan, S.G., Zhao, X.M., 2015. Petrological and geochemical features of the Jingtieshan banded iron formation (BIF): a unique type of BIF from the Northern Qilian Orogenic Belt, NW China. J. Asian Earth Sci. 113, 1218–1234.

Yang, X.Q., Zhang, Z.H., Santosh, M., Li, C., Liang, T., 2018. Hydrothermal copper mineralization in the Mesoproterozoic Huashugou banded iron formation, Northwest China: characteristics, timing of formation and genesis. Ore Geol. Rev. 102, 776–790.

Zhai, M.G., Santosh, M., 2013. Metallogeny of the North China Craton: Link with secular changes in the evolving Earth. Gondwana Res. 24, 275–297.

Zhai, M.G., Sills, J.D., Windley, B.F., 1990b. Metamorphic mineral and metamorphism of the Anshan Group in Anshan-Benxi area, Liaoning. Acta Petrol. Mineral. 9, 148–158 (in Chinese with English abstract).

Zhai, M.G., Windley, B.F., Sills, J.D., 1990a. Archaean gneisses, amphibolites and banded iron–formations from the Anshan area of Liaoning Province, NE China: their geochemistry, metamorphism and petrogenesis. Precambr. Res. 46, 195–216.

Zhai, M.G., Windley, B.F., 1990. The Archaean and early Proterozoic banded iron formations of North China: their characteristics, geotectonic relations, chemistry and implications for crustal growth. Precambr. Res. 48, 267–286.

Zhang, Z.C., Hou, T., Santosh, M., Li, H.M., Li, J.W., Zhang, Z.H., Song, X.Y., Wang, M., 2014. Spatio–temporal distribution and tectonic settings of the major iron deposits in China: an overview. Ore Geol. Rev. 57, 247–263.

Zhang, Y., Shao, Y.J., Wu, C.D., Chen, H.Y., 2017. LA–ICP–MS trace element geochemistry of garnets: constraints on hydrothermal fluid evolution and genesis of the Xinqiao Cu–S–Fe–Au deposit, eastern China. Ore Geol. Rev. 86, 426–439.

Zhang, Z.M., Yang, Y., Zhang, J.X., 2000. The compositional zoning of garnet in eclogitefrom western segment of Altyn Tagh, northwestern China and its dynamic significance. Chin. Sci. Bull. 45, 79–83.

Zhang, L.C., Zhai, M.G., Wan, Y.S., Guo, J.H., Dai, Y.P., Wang, C.L., Liu, L., 2012. Study of Precambrian BIF–iron deposits in North China Craton: progress and questions. Acta Petrol. Sin. 28, 3431–3445 (in Chinese with English abstract).

Zhang, L.C., Wang, C.L., Zhu, M.T., Huang, H., Peng, Z.D., 2016. Formation ages and environments of Early Precambrian banded iron formation in the North China Craton. In: Zhai, M.G. (Ed.), Main Tectonic Events and Metallogeny of the North China Craton. Springer, pp. 85–103.

Zhang, Q.S., Yang, Z.S., 1988. Early Crust and Mineral Deposits of Liaodong Peninsula. Geological Publishing House, Beijing, pp. 218–450 (in Chinese).

Zhao, B., Li, T.J., 1980. A preliminary study on the mechanism and physico–chemical conditions of the formation of the Gongchangling rich iron deposit. Geochimica 9, 333–344 (in Chinese with English abstract).

Zhao, G.C., Wilde, S.A., Cawood, P.A., Lu, L.Z., 1998. Thermal Evolution of Archean Basement Rocks from the Eastern Part of the North China Craton and Its Bearing on Tectonic Setting. Int. Geol. Rev. 40, 706–721.

Zhao, G.C., Zhai, M.G., 2013. Lithotectonic elements of Precambrian basement in the North China Craton: review and tectonic implications. Gondwana Res. 23, 1207–1240.

Zhao, G.C., Sun, M., Wilde, S., 2003. Major tectonic units of the North China Craton and their Paleoproterozoic assembly. Sci. China (Ser. D) 46, 23–38.

Zhao, G.C., Sun, M., Wilde, S.A., Li, S.Z., 2005. Late Archean to Paleoproterozoic evolution of the North China Craton: key issues revisited. Precambr. Res. 136, 177–202.

Zhao, G.C., Cawood, P.A., Li, S.Z., Wilde, S.A., Sun, M., Zhang, J., He, Y.H., Yin, C.Q., 2012. Amalgamation of the North China Craton: key issues and discussion. Precambr. Res. 222–223, 55–76.

Zhao, B., Wang, S.Y., Li, T.J., 1979. The origin of migmatite granite and its relationship with iron deposit: an experimental study. Geochimica 8, 211–221 (in Chinese with English abstract).

Zhao, G.M., Wilde, S.A., Cawood, P.A., Sun, M., 2001. Archean blocks and their boundaries in the North China Craton: lithological, geochemical, structural and P-T path constraints and tectonic evolution. Precambr. Res. 107, 45–73.

Zhou, S.T., 1994. Geology of Banded Iron Formations in Anshan-Benxi Area. Geological Publishing House, Beijing, pp. 278 (in Chinese).

Zhu, K., Liu, Z.H., Xu, Z.Y., Wang, X.A., Liu, J.X., 2016. Genesis of altered rocks and high-grade iron ore in Gongchangling iron deposit. Earth Sci. Front. 23 (5), 235–251.